Tuning the Intrinsic Anisotropy with Disorder in the CaKFe4As4 Superconductor

Tuning the Intrinsic Anisotropy with Disorder in the $CaKFe_4As_4$ Superconductor

D. Torsello,[1,2,*] G.A. Ummarino,[1,3] J. Bekaert,[4] L. Gozzelino,[1,2] R. Gerbaldo,[1,2] M.A. Tanatar,[5,6] P.C. Canfield,[5,6] R. Prozorov,[5,6] and G. Ghigo[1,2]

[1] *Department of Applied Science and Technology, Politecnico di Torino, Torino 10129, Italy*
[2] *Istituto Nazionale di Fisica Nucleare, Sezione di Torino, Torino 10125, Italy*
[3] *National Research Nuclear University MEPhI (Moscow Engineering Physics Institute), Moskva 115409, Russia*
[4] *Department of Physics, University of Antwerp, Groenenborgerlaan 171, Antwerp B-2020, Belgium*
[5] *Ames Laboratory, Iowa State University, Ames, Iowa 50011, USA*
[6] *Department of Physics & Astronomy, Iowa State University, Ames, Iowa 50011, USA*

(Received 9 January 2020; revised manuscript received 14 April 2020; accepted 28 May 2020; published 18 June 2020)

We report on the anisotropy of the London penetration depth of $CaKFe_4As_4$, discussing how it relates to its electronic structure and how it modifies under introduction of disorder, both chemically induced (by Ni substitution) and irradiation induced (by 3.5-MeV protons). Indeed, $CaKFe_4As_4$ is particularly suitable for the study of fundamental superconducting properties due to its stoichiometric composition, exhibiting clean-limit behavior in the pristine samples and having a fairly high critical temperature, $T_c \approx 35$ K. The London penetration depth λ_L is measured with a microwave-coplanar-resonator technique that allows us to deconvolve the anisotropic contributions $\lambda_{L,ab}$ and $\lambda_{L,c}$ and obtain the anisotropy parameter $\gamma_\lambda = \lambda_{L,c}/\lambda_{L,ab}$. The $\gamma_\lambda(T)$ found for the undoped pristine sample is in good agreement with previous literature and is here compared to *ab initio* density-functional-theory and Eliashberg calculations. The dependence of $\gamma_\lambda(T)$ on both chemical and irradiation-induced disorder is discussed to highlight which method is more suitable to decrease the direction dependence of the electromagnetic properties while maintaining a high critical temperature. Lastly, the relevance of an intrinsic anisotropy such as γ_λ on application-related anisotropic parameters (critical current, pinning) is discussed in light of the recent employment of $CaKFe_4As_4$ in the production of wires.

DOI: 10.1103/PhysRevApplied.13.064046

I. INTRODUCTION

One of the reasons why iron-based superconductors (IBSs) are very interesting for applications is their low anisotropy [1]. Despite their complex electronic structure, when compared to the cuprate family of high-temperature superconductors, their properties relevant to transport applications stand out as almost isotropic. However, a closer look reveals some unconventional behavior of the anisotropy of both the penetration depth ($\gamma_\lambda = \lambda_c/\lambda_{ab}$) and the upper critical field ($\gamma_H = H_{c2,ab}/H_{c2,c}$) and of their temperature dependence.

In conventional low-temperature single-band BCS superconductors, both γ_λ and γ_H are temperature independent and are equal; therefore, the temperature dependence of the anisotropy has been considered for a long time as a signature of multiband conductivity, since it is the typical behavior of MgB_2 [2,3]. Conversely, it has recently been pointed out that it can also originate from anisotropy of the order parameter, such as non-*s*-wave character [4]. For the same historical reason, it is a common belief that γ_λ and γ_H, when temperature dependent, should vary in opposite ways. If γ_λ increases with increasing temperature, γ_H should decrease (as in MgB_2 [3]) or vice versa (as in the 122 family of IBSs [5,6]). The recent observation of both anisotropies increasing with increasing temperature in the case of $CaKFe_4As_4$ (CaK1144) [7] has challenged this view and stimulated further theoretical and experimental investigations.

Moreover, the increasing interest in IBSs for the production of tapes, wires, and coated conductors requires a full characterization of their anisotropic transport and pinning properties, which have been shown to be strongly related to intrinsic anisotropies such as γ_λ [8]. Specifically, the anisotropy parameter that enters the anisotropic Ginzburg-Landau (AGL) scaling relation for the angle-dependent critical current has been shown to behave just as γ_λ for MgB_2 [9] and Fe(Se,Te) [8] and as γ_H for $Ba(Fe,Co)_2As_2$ [10]. In addition, vortex pinning and anisotropy place fundamental restrictions on the current-carrying capability of materials [11] and therefore a way to engineer them is required.

*daniele.torsello@polito.it

In this work, we determine experimentally the temperature dependence of the London-penetration-depth anisotropy in $CaKFe_4As_4$ crystals and how it is modified by chemical and ion-irradiation-induced disorder. Chemical disorder is studied by Ni for Fe substitution, which increases electron doping, whereas 3.5-MeV proton irradiation produces pointlike defects and small clusters [12]. The experimental data for the undoped pristine case are compared to *ab initio* density-functional-theory (DFT) and multiband-Eliashberg-theory calculations. The relevance of an intrinsic anisotropy such as γ_λ on application-related anisotropic parameters (critical current, pinning) is also discussed in light of the recent employment of CaK1144 in the production of wires [13] and tapes [14]. In this respect, the ability to tune the anisotropy with disorder is a valuable tool for applications and in the paper we discuss which method between doping and irradiation is more suitable to decrease the direction dependence of the electromagnetic properties while maintaining a high critical temperature.

II. EXPERIMENTAL TECHNIQUES AND THEORETICAL METHODS

A. Crystals preparation

High-quality single crystals of $CaK(Fe_{1-x}Ni_x)_4As_4$ with analyzed doping levels of $x = 0$, $x = 0.014$, and $x = 0.037$, are grown by high-temperature solution growth out of FeAs flux [15]. The samples are cleaved and reduced to the form of thin rectangular plates with thicknesses ranging from 3 to about 35 μm, in the direction of the c axis of the crystals, and widths and lengths at least one order of magnitude larger.

B. Penetration-depth measurements

The London penetration depth is measured by means of a coplanar-waveguide-resonator (CPWR) technique that has already been applied to study other IBS crystals [16–19]. The resonator consists of an $YBa_2Cu_3O_{7-x}$ coplanar waveguide to which the sample is coupled. The whole resonance curve is recorded with a vector-network analyzer, making it possible to track resonant-frequency shifts and variations of the unloaded quality factor. This procedure gives access to the absolute value of the penetration depth and its temperature dependence after a calibration procedure is performed (full details in Ref. [20]).

The sample is positioned on top of the central strip of the resonator in a region where the electric field vanishes, in a configuration with the rf magnetic field parallel to the *ab* planes of the sample, i.e., to its broad face. Due to the finite size of the crystal and the consequent demagnetization field, the measurements yield an effective penetration depth λ_L that is a combination of the main components $\lambda_{L,ab}$ and $\lambda_{L,c}$. This combination depends on the geometry of the sample under consideration and for this reason both components can be retrieved by measuring samples with significantly different aspect ratios.

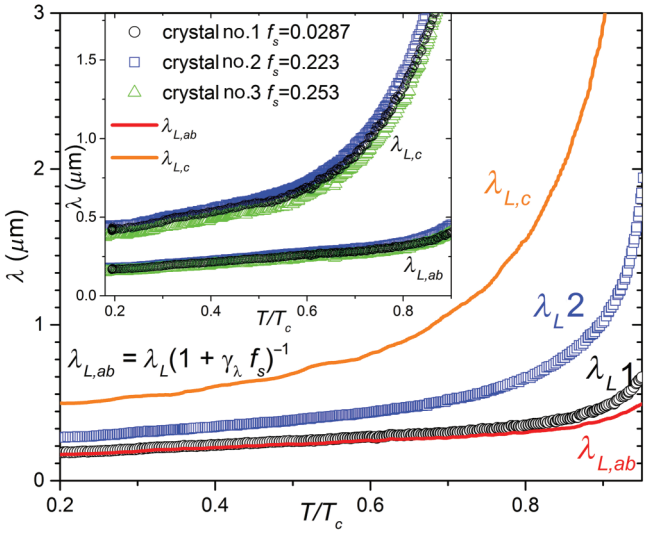

FIG. 1. The effective penetration depth of two crystals with largely different shape factors and the resulting deconvolved $\lambda_{L,ab}$ and $\lambda_{L,c}$ contributions. The inset shows the best collapse of the $\lambda_{L,ab}$ and $\lambda_{L,c}$ data from three crystals, resulting in the anisotropy factor discussed in Fig. 4.

Accordingly, and on the hypothesis that $\lambda_{L,ab} < c$ and $\lambda_{L,c} < a, b$ (where $2c$, $2a$, and $2b$ are, respectively, the thickness, width, and length of the samples), the fraction of volume penetrated by the field can be estimated as $\lambda_{L,ab}/c + \lambda_{L,c}/a + \lambda_{L,c}/b$. Thus, the measured penetration depth can be expressed as

$$\lambda_L = \lambda_{L,ab} + f_s \lambda_{L,c}, \tag{1}$$

where $f_s = c(1/a + 1/b)$ is the sample shape factor.

An example of the λ_L deconvolution procedure for pristine undoped CaK1144 is given in Fig. 1, where $\lambda_{L,ab}$ and $\lambda_{L,c}$ are extracted from the comparison of two crystals with very different shape factors (one order of magnitude). To improve precision, further crystals can be analyzed: we show in the inset of Fig. 1 the best collapse of the $\lambda_{L,ab}$ and $\lambda_{L,c}$ data from three crystals, resulting in the $\gamma_\lambda(T)$ reported in Fig. 4.

C. Proton irradiation

The 3.5-MeV proton irradiation is performed at the CN facility of the Legnaro National Laboratories (LNL) of the Italian National Institute for Nuclear Physics (INFN), with the beam parallel to the c axis of the crystals. The range of protons into the material is estimated to be about 66 μm by Monte Carlo simulations performed with the PHITS [21] and SRIM [22] codes within the Kinchin-Pease approach. The thickness of all the investigated samples is much smaller than this value (maximum 35 μm), ensuring that

proton implantation is avoided and that a rather homogeneous distribution of defects is achieved. The CPWR measurements are carried out before and after each irradiation session.

D. DFT calculations

DFT calculations, as implemented in ABINIT [23], are performed to obtain the Fermi surface of $CaKFe_4As_4$. We use the Perdew-Burke-Ernzerhof (PBE) functional, in combination with projector-augmented-wave (PAW) atomic potentials, taking into account Ca $3s^2 3p^6 4s^2$, K $3s^2 3p^6 4s^1$, Fe $3s^2 3p^6 3d^6 4s^2$, and As $3d^{10} 4s^2 4p^3$ as valence states. An energy cutoff of 15 Hartree for the plane-wave basis is used together with a $20 \times 20 \times 6$ Γ-centered Monkhorst-Pack **k**-point grid. The crystal structure is relaxed so that the forces on each atom are below 1 meV/Å, yielding lattice parameters $a = 3.94$ Å and $c = 11.82$ Å.

The Fermi surface consists of five bands centered around Γ with a hole character and three bands centered around M with an electron character [Fig. 2(a)]. One of the bands centered around Γ (the outer one) is much larger and more warped than the other four, suggesting that the system can be essentially described by a simplified three-component model (one equivalent electron band and two equivalent hole bands, one of which is the outer Γ band). To further characterize the superconducting components, we calculate the band-resolved density of states (DOS) using Gaussian integration of the DFT Kohn-Sham eigenvalues with a width of 0.1 eV [Fig. 2(b)]. The behavior of the band-resolved DOS supports the choice to employ a three-component model and allows us to calculate the component-resolved DOS at the Fermi level $N_i(0)$ (Tables I and II).

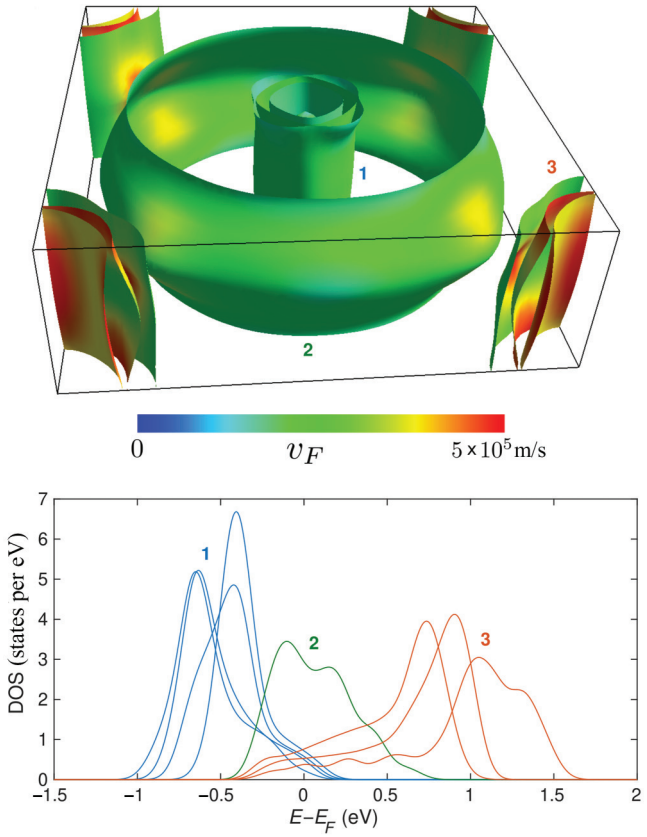

FIG. 2. (a) The Fermi surface of $CaKFe_4As_4$ calculated using DFT, depicted in the Γ-centered Brillouin zone. (b) The band-resolved electronic density of states around the Fermi level. A total of eight bands are present, their characteristics suggesting that the system can essentially be described by a simplified three-component model.

TABLE I. The parameters for the three-component model.

Component	N (eV^{-1})	$\Delta(0)$ (meV)	$\langle v_{F,a}\rangle$ ($=\langle v_{F,b}\rangle$) (m/s)	$\langle v_{F,c}\rangle$ (m/s)
1	2.03	11	1.08×10^5	0.21×10^5
2	2.94	7	1.16×10^5	0.90×10^5
3	1.67	11	2.08×10^5	0.37×10^5

For each of the three components, we also calculate the average Fermi velocities in the ab and c directions (Tables I and II) from the DFT Kohn-Sham eigenvalues (ϵ_{KS}), using $\mathbf{v}_F = \hbar^{-1}\nabla_{\mathbf{k}}\epsilon_{KS}|_{\epsilon_{KS}=E_F}$, and subsequently averaging over the ab and c directions to capture the anisotropy.

E. Eliashberg modelling

The Eliashberg theory has been proven very helpful in the interpretation of experimental data for IBSs due to the possibility of taking into account the spin-fluctuation pairing mechanism and the multiband nature of these materials [24,25]. The London penetration depth can easily be calculated from the solution of the imaginary-axis version of the Eliashberg equations. As suggested by the DFT calculations, we employ a three-band model with pairing provided by antiferromagnetic spin fluctuations. The coupling constants are determined to reproduce the experimental critical temperature and the gap values measured by angle-resolved photoemission spectroscopy (ARPES) [26]. Figure 3 shows the temperature dependence of the energy gaps obtained by the solution of the imaginary-axis Eliashberg equations.

TABLE II. The parameters for the two-component model [4].

Component	N (eV^{-1})	$\Delta(0)$ (meV)	$\langle v_{F,a(b)}\rangle$ (m/s)	$\langle v_{F,c}\rangle$ (m/s)
1	4.97	11	1.12×10^5	0.60×10^5
2	1.67	9	2.08×10^5	0.37×10^5

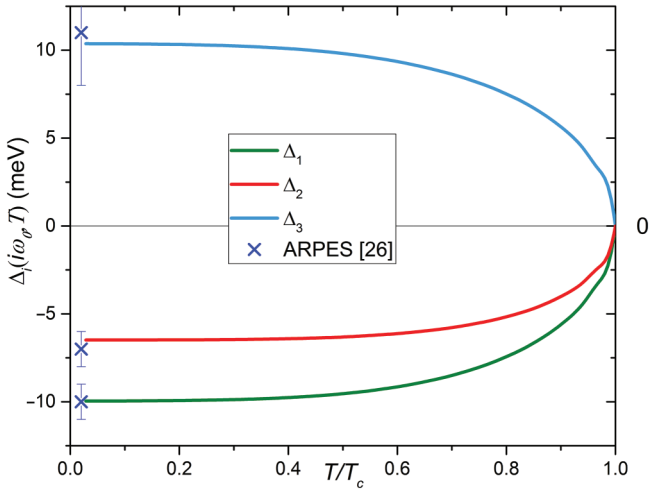

FIG. 3. The temperature dependence of the first value of the energy gaps of $CaKFe_4As_4$ obtained by the solution of the imaginary-axis Eliashberg equations. The crosses give the experimental ARPES data [26] for comparison.

All the details for the Eliashberg procedure to fix free parameters and calculate the London penetration depth are given elsewhere [24,27]. In this specific case though, we do not consider the plasma frequency on each band as a free parameter but we obtain it from first principles.

We use a simplified model in which gap anisotropy is not taken into account. However, it is still possible to evaluate anisotropic properties by employing the anisotropic average Fermi velocity on each band obtained by DFT. In fact, the London penetration depth calculated by the Eliashberg theory can be written as

$$[\lambda_L^{\mathrm{El}}(T)]^{-2} = \sum_{i=1}^{3} \left(\frac{\omega_{p,i}}{c}\right)^2 \pi T \Xi_i, \tag{2}$$

where $\omega_{p,i}$ is the bare plasma frequency on the ith band, which is related to the London penetration depth by $\omega_p = c/\lambda_L(0)$ only in the case of a clean uniform superconductor at $T = 0$ and in the presence of negligible Fermi-liquid effects. If this is not the case, this relation is modified as $\omega_p^{\mathrm{sf}} = c/\lambda_L(0)$, where ω_p^{sf} is the renormalized superfluid plasma frequency [28]. Ξ_i gives the renormalization of the ith band estimated by the Eliashberg theory through the gap functions $\Delta_i(i\omega_n)$ and the renormalization functions $Z_i(i\omega_n)$ solution of the imaginary-axis Eliashberg equations as

$$\Xi_i = \sum_{n=-\infty}^{+\infty} \frac{\Delta_i^2(\omega_n) Z_i^2(\omega_n)}{[\omega_n^2 Z_i^2(\omega_n) + \Delta_i^2(\omega_n) Z_i^2(\omega_n)]^{3/2}}. \tag{3}$$

The bare, band-resolved, and direction- (α and β) dependent plasma frequencies can be computed from first principles [28] (with the parameter values shown in Table I):

$$\omega_{p,i}^{\alpha\beta} = \sqrt{\frac{8\pi e^2}{\epsilon_o} N_i(0) \langle v_{F,\alpha} v_{F,\beta} \rangle_{FS_i}}, \tag{4}$$

where α and β are ab or c, and $v_{F,ab}^2 = v_{F,a}^2 + v_{F,b}^2$. Accordingly, a bare anisotropy parameter can be calculated in the zero-temperature limit as $\gamma_\lambda^{\mathrm{bare}} = \omega_p^{ab}/\omega_p^c$, as discussed by Kogan [2], while a renormalized anisotropy parameter can be obtained through Eqs. (2) and (3) as $\gamma_\lambda^{\mathrm{El}} = \lambda_{L,c}^{\mathrm{El}}/\lambda_{L,ab}^{\mathrm{El}}$. The latter can also be studied as a function of the temperature, starting from the temperature dependence of the gaps calculated within the Eliashberg approach.

III. RESULTS AND DISCUSSION

A. Pristine undoped CaK1144

The experimental $\gamma_\lambda(T)$ for the pristine undoped CaK1144 case is shown in Fig. 4, where it is also compared to literature data from muon spin rotation (μSR) experiments [7] and to calculated values. Experimental data are shown up to the reduced temperature at which all the approximations discussed in Secs. II B are valid. The qualitative behavior from the two experimental techniques is comparable, with higher values in the CPWR case that can be ascribed to higher sample quality or to the higher frequency of the experimental probe, which

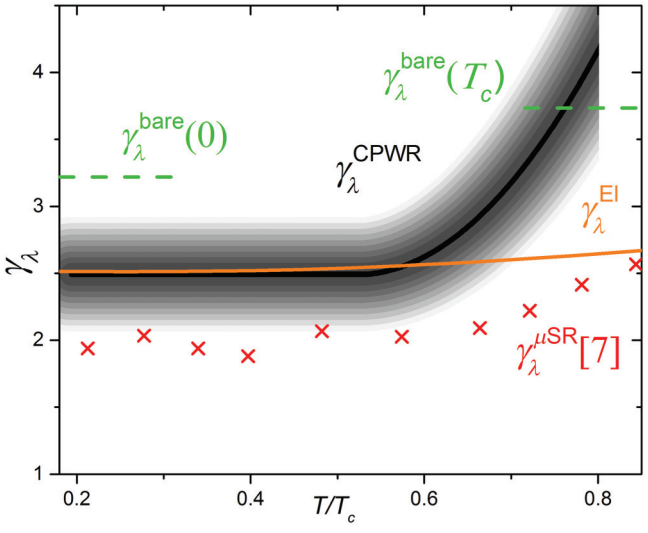

FIG. 4. The experimental anisotropy for the pristine undoped CaK1144, $\gamma_\lambda^{\mathrm{CPWR}}$ (black solid line) with its estimated uncertainty (shaded area) compared to μSR data (red crosses) [7] and theoretical expectations, discussed in the text. The $\gamma_\lambda^{\mathrm{bare}}$ values (green) at $T = 0$, T_c are derived directly by *ab initio* DFT calculations, while $\gamma_\lambda(T)^{\mathrm{El}}$ (orange solid line) takes into account the normalization given by the Eliashberg approach.

might reduce the scattering contribution [29]. As discussed above, due to the stoichiometric composition of undoped CaK1144, it has been possible to compute the bare low-temperature anisotropy parameter from first principles as well as the renormalized one with its temperature dependence on the hypothesis that the gaps are isotropic. Both theoretical low-temperature values are comparable with our experimental data: the bare value is slightly larger, whereas the renormalized one is in remarkable agreement. The temperature dependence of the renormalized $\gamma_\lambda^{\mathrm{El}}$ shows a modest upward curvature, reminiscent of the experimental behavior albeit quantitatively much smaller. From the comparison between the experimental and theoretical $\gamma_\lambda(T)$, it can be deduced that the gap and the full Fermi-surface anisotropies (not included in the model) probably play a prominent role in the temperature dependence of the anisotropy parameter. This can be easily deduced by comparing the limiting behavior of $\gamma_\lambda(T)$ for $T \to 0$ and $T \to T_c$ discussed by Kogan *et al.* [2]. While for the low-temperature limit only the Fermi velocities play a role, approaching the critical temperature a parameter that describes gap anisotropy (Ω) enters the equation. This model has been recently extended to allow an approximate treatment of two-component systems with anisotropic Fermi surfaces, starting from a few input parameters [4] that can easily be estimated starting from the DFT and Eliashberg data discussed above. For this purpose, from our DFT data, we group the several band contributions into just two components, yielding the partial DOS and direction-resolved Fermi velocities of each component, and from the Eliashberg calculations we obtain an estimate of the gaps in the two-component model by simply averaging the two contributions on the Γ bands. With the values summarized in Table II, we obtain, from Eqs. (31) and (32) in Ref. [4], that both γ_λ and γ_H increase with increasing temperature and that the variation is stronger for H_{c2} than for λ_L, as experimentally observed [7] [$\gamma_\lambda(0)/\gamma_\lambda(T_c) \simeq 0.87$ and $\gamma_H(0)/\gamma_H(T_c) \simeq 0.8$]. As a reference, we add to Fig. 4 the value of $\gamma_\lambda^{\mathrm{bare}}$ at T_c, as $\gamma_\lambda^{\mathrm{bare}}(0)/0.87$. This value is close to the experimental ones at high temperatures, suggesting that indeed the Fermi-surface anisotropy is crucial to address γ_λ when approaching T_c.

B. Disorder dependence of γ_λ

Disorder is a valuable tool for tuning anisotropy. Here, we study the effects of two types of disorder: chemical substitution (Ni for Fe) and 3.5-MeV-proton-irradiation-induced defects. This latter source of disorder produces mostly pointlike defects (vacancies, interstitials, and Frenkel pairs) and small collision cascades with an expected size of a few nanometers [12], which produce isotropic scattering of carriers and are then expected to reduce the anisotropy [2]. As is visible from Fig. 5, both typologies of disorder reduce the overall anisotropy but

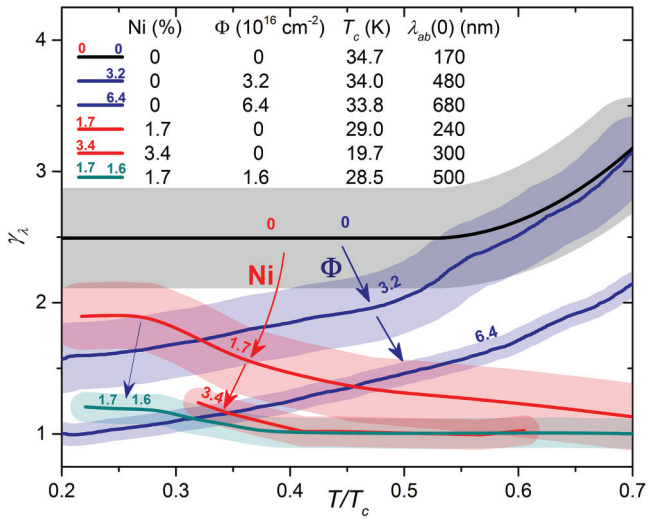

FIG. 5. The disorder dependence of the penetration-depth anisotropy. Disorder is introduced by chemical substitution of Ni for Fe (red) and 3.5-MeV-proton-irradiation-induced defects (blue) or a combination of the two (cyan).

the temperature dependence is affected in opposite ways. With an increasing irradiation fluence (and therefore defect concentration), $\gamma_\lambda(T)$ preserves its qualitative temperature behavior: increasing with temperature for the undoped case and decreasing with temperature for the 1.7%-Ni-doped case. On the other hand, Ni substitution changes the temperature evolution from increasing to decreasing.

This experimental evidence should be interpreted in light of the fact that the substitution of Fe with Ni provides electron doping and its main consequence is to shift the Fermi level. However, these dopant ions also cause substantial scattering [29] (i.e., pair-breaking), just as does the introduction of defects through irradiation.

We find a decrease of anisotropy at low temperature both in irradiated and substituted samples, so we can ascribe this modification to the increase of scattering (a parameter not included in the models previously discussed). On the other hand, in the previous section, by comparing the two models, we discuss how, in the $T \to T_c$ limit, the gap anisotropy is predominant in determining γ_λ . Therefore, the observed change of temperature dependence of γ_λ as a consequence of Ni substitution is compatible with the expected modification of the band and gap structure. Moreover, in combination with the decrease of the critical temperature due to Ni doping or ion irradiation, it is possible to discuss which method (or which combination) could be more advantageous to tune the anisotropy for a specific application.

C. Relevance for applications

In the production of tapes, wires, and coated conductors, the nature of grain boundaries and the anisotropy of

the critical current are critical aspects. If the anisotropy of the material is too high and if a precise grain-boundary orientation is required, three-dimensionally controlled crystallite growth is needed, resulting in complicated fabrication processes and therefore high costs [30]. IBSs have the advantage, with respect to the cuprates, that the critical angle for grain orientation is quite large. This fact allows a wide space for improvement of the intergrain properties through the optimization of production processes such as texturing and application of pressure [31]. The intrinsic characteristics of these materials are not a fundamental limitation in this respect. This is especially true when considering the specific case of coated conductors, which, although still a young technology, are promising with regard to achieving the critical-current densities needed for practical applications [32]. However, the intragrain properties, on the other hand, are not intrinsically as excellent as in the cuprates and their optimization is pivotal for applications. For this reason, the study of single-crystal properties (where grain boundaries are absent) and the investigation of approaches for their optimization are particularly relevant. Recently, a study on proton irradiation of single crystals of $CaKFe_4As_4$ has shown that the critical current of this material can be strongly enhanced by introducing pointlike defects [33], making this material particularly interesting for applications. Moreover, despite the fact that IBSs are much less anisotropic than the cuprates, anisotropy values in the range of 2–5 can still result in a decrease of practical values of the superconducting parameters when external or stray fields are present (e.g., the engineering critical current of a coated conductor employed in the assembly of magnets), making the optimization of anisotropy a strong requirement for applications.

When flux-pinning models are considered to explain the field-angular dependence and anisotropy of the critical-current density in IBSs, it turns out explicitly that the penetration-depth anisotropy plays a role, together with the coherence-length anisotropy [34]. In particular, γ_λ directly enters into the elementary pinning force through the line energy term. The penetration-depth anisotropy appears in the expressions for $j_c(\theta)$, with a relative weight depending on the pinning regime, the shape of the defects, and, in general, on the optimization of the matching between the vortex lattice and the defect matrix.

In the analysis of the angular dependence of the critical current $J_c(\theta)$, a valuable tool is the AGL approach [35], which allows one to scale $J_c(\theta)$ with an effective magnetic field. The scaling involves an anisotropy parameter γ_s that, for a simple clean single-band case, should be the effective mass anisotropy that also coincides with the low-temperature limit of the penetration-depth anisotropy $\gamma_s = \gamma_m = \sqrt{m_c/m_{ab}} = \gamma_\lambda$.

Here, we want to stress that γ_λ does not take pinning into account (since it is measured below the critical field for vortex penetration) but only the properties of the carriers and the way they interact with their surroundings, and for this reason we describe it as "intrinsic". Moreover, it might differ below T_c from the $\sqrt{m_c/m_{ab}}$ value of the clean system due to scattering and since it also depends on the fine details of the pairing, multiband nature, and structure of the Fermi surface [4].

However, the AGL-scaling approach has also been shown to work well for multiband systems [34], with γ_s found to follow the temperature behavior of intrinsic anisotropies such as γ_λ for MgB_2 [9] and Fe(Se,Te) [8] and as γ_H for $Ba(Fe,Co)_2As_2$ [10]. A similar relation between the AGL anisotropy and the intrinsic anisotropy of the penetration depth, although only qualitative, has also been observed for other systems such as the 1111 [36] and the 111 [37] IBS families. All these observations, together with the quantitative relations that are valid for simplified and limiting cases, strongly suggest that the intrinsic anisotropy has a strong correlation with the practical anisotropies to be optimized for applications. A correct application of the AGL scaling with γ_s estimated by γ_λ could yield useful information about the pinning regime in the material [8], another essential aspect for applications. For these reasons, the study of γ_λ, and of the possible approaches to tuning it, acquire particular relevance for the application-oriented investigation of IBSs.

In light of the above discussion, the experimental data summarized in Fig. 5 suggest that ion irradiation might be advantageous with respect to chemical doping for tuning the anisotropy. The low-temperature value of γ_λ can be reduced significantly with a relatively low proton dose that has a minimal influence on the critical temperature [$\gamma_\lambda(T \simeq 5K) \simeq 1$, with a decrease of T_c of less than 1 K; see the tabulated key in Fig. 5]. Moreover, it has been shown that ion irradiation has a beneficial effect on the critical current of CaK1144 tapes: 3-MeV proton irradiation with a dose yielding a comparable decrease of T_c to the one discussed here has resulted in an increase of J_c close to 500% at 2 K [38]. Comparable results have also been found on single crystals from the same source as in this study, irradiated with 3-MeV protons [33]. Interestingly, the irradiation dose that has yielded the maximum increase of the critical-current density caused a reduction of T_c very close to the one we observe in the crystals that show a γ_λ at low temperature equal to 1 (isotropic behavior). It should be noted that the decrease of the anisotropy is achieved at the expense of an increased absolute value of λ_L. In principle, this increase is detrimental for high currents and thermal fluctuations but, as just discussed, the critical current is found to increase due to the contribution of additional pinning. Also, thermal fluctuations are not expected to play a critical role in applications, since a fourfold increase of λ_L would result in a width of the critical-fluctuations regime smaller than 1 K (estimated using the Ginzburg number [39]), far from the expected working conditions.

The combination of all these results (namely, the small decrease of T_c, the increase of the penetration depth, and the advantageous increase of the critical current and decrease of anisotropy) strongly indicates that proton irradiation might be extremely useful in the optimization of $CaKFe_4As_4$ properties for practical applications. In this respect, it is noteworthy that several steps toward the applicability of ion irradiation in the commercial production of coated conductors have recently been reported [40–42]. The proton irradiation used in this work and the irradiation with larger ions at moderate energies compatible with commercial production share a similar typology of defects: in both cases, small clusters and point defects are introduced.

In addition, it has been pointed out that keeping the stoichiometric composition of CaK1144 is by itself a strong advantage in the production process of wires and tapes [11] and ion irradiation allows us to tune several properties while keeping the stoichiometry fixed.

IV. CONCLUSIONS

We report on the anisotropy of the London penetration depth of $CaKFe_4As_4$, experimentally evaluated by means of a microwave CPWR technique, compared to expectations based on *ab initio* DFT calculations and Eliashberg modeling. The penetration-depth anisotropy found for the undoped pristine crystals is in fairly good agreement with previous μSR experiments [7] and with theoretical predictions. Indeed, it results from Fig. 4 that both experimental evaluations of $\gamma_\lambda(T)$ (from CPWR and μSR) and calculated ones (from bare and renormalized DFT results, in three-gap and two-gap approximations) show an increase with temperature and comparable absolute values. In more detail, a remarkable agreement is found between the experimental low-temperature anisotropy and the value calculated from DFT with an Eliashberg renormalization within a three-band approach [$\gamma_\lambda(0) \approx 2.5$]. On the contrary, the experimental $\gamma_\lambda(T)$ cannot be reproduced well at temperatures approaching T_c by the Eliashberg model, in which the gap and the Fermi-surface anisotropies are not accounted for. A simple two-component model that includes the Fermi-surface anisotropy [4] yields a stronger temperature dependence of the anisotropy parameter, suggesting that a fully anisotropic Eliashberg treatment—which is beyond the scope of this work—could fully capture the experimentally observed behavior.

The dependence of $\gamma_\lambda(T)$ on both chemical and irradiation-induced disorder has been studied. Both kinds of disorder result in a general decrease of the intrinsic anisotropy, but with distinctive features. While irradiation defects mainly act at low temperatures, preserving the increasing temperature dependence, doping with Ni on the Fe site causes a decreasing $\gamma_\lambda(T)$ temperature dependence. This fact, in combination with the employed models, suggests that Ni substitution modifies the electronic and gap structure more strongly than irradiation-induced defects, while interband scattering is the most likely candidate to explain the decrease of γ_λ at low temperature.

We obtain, particularly with a combination of doping and irradiation, crystals with virtually isotropic behavior. On the other hand, if one aims at discussing which method is the most convenient to decrease $\gamma_\lambda(T)$ in view of practical applications, doping and irradiation effects on the other key parameters should be taken into account: doping causes a fast decrease of the critical temperature, while irradiation mainly affects $\lambda_{L,ab}(0)$. In the case of tapes or wires, the second method could be preferred, since it simultaneously assures low anisotropy, a very low decrease of T_c, and a huge increase of the critical-current density through flux pinning.

ACKNOWLEDGMENTS

This work was partially supported by the Italian Ministry of Education, University and Research (Project PRIN "HIBiSCUS," Grant No. 201785KWLE). J.B. acknowledges the support of a postdoctoral fellowship of the Research Foundation-Flanders (FWO). The computational resources and services used for the first-principles calculations in this work were provided by the VSC (Flemish Supercomputer Center), funded by the FWO and the Flemish Government—department EWI. Work done at Ames Laboratory was supported by the U.S. Department of Energy, Office of Basic Energy Science, Division of Materials Sciences and Engineering. Ames Laboratory is operated for the U.S. Department of Energy by Iowa State University under Contract No. DE-AC02-07CH11358. G.A.U. acknowledges support from the MEPhI Academic Excellence Project (Contract No. 702.a03.21.0005).

[1] M. Putti *et al.*, New Fe-based superconductors: Properties relevant for applications, Supercond. Sci. Technol. **23**, 034003 (2010).

[2] V. G. Kogan, Macroscopic anisotropy in superconductors with anisotropic gaps, Phys. Rev. B **66**, 020509 (2002).

[3] J. D. Fletcher, A. Carrington, O. J. Taylor, S. M. Kazakov, and J. Karpinski, Temperature-Dependent Anisotropy of the Penetration Depth and Coherence Length of MgB_2, Phys. Rev. Lett. **95**, 097005 (2005).

[4] V. G. Kogan, R. Prozorov, and A. E. Koshelev, Temperature-dependent anisotropies of upper critical field and London penetration depth, Phys. Rev. B **100**, 014518 (2019).

[5] R. Khasanov, D. V. Evtushinsky, A. Amato, H.-H. Klauss, H. Luetkens, C. Niedermayer, B. Büchner, G. L. Sun, C. T. Lin, J. T. Park, D. S. Inosov, and V. Hinkov, Two-Gap Superconductivity in $Ba_{1-x}K_xFe_2As_2$: A Complementary

Study of the Magnetic Penetration Depth by Muon-Spin Rotation and Angle-Resolved Photoemission, Phys. Rev. Lett. **102**, 187005 (2009).

[6] M. A. Tanatar, N. Ni, C. Martin, R. T. Gordon, H. Kim, V. G. Kogan, G. D. Samolyuk, S. L. Bud'ko, P. C. Canfield, and R. Prozorov, Anisotropy of the iron pnictide superconductor $Ba(Fe_{1-x}Co_x)_2As_2$ ($x = 0.074$, $T_c = 23$K), Phys. Rev. B **79**, 094507 (2009).

[7] R. Khasanov, W. R. Meier, S. L. Bud'ko, H. Luetkens, P. C. Canfield, and A. Amato, Anisotropy induced vortex lattice rearrangement in $CaKFe_4As_4$, Phys. Rev. B **99**, 140507 (2019).

[8] K. Iida, J. Hänisch, E. Reich, F. Kurth, R. Hühne, L. Schultz, B. Holzapfel, A. Ichinose, M. Hanawa, I. Tsukada, M. Schulze, S. Aswartham, S. Wurmehl, and B. Büchner, Intrinsic pinning and the critical current scaling of clean epitaxial Fe(Se, Te) thin films, Phys. Rev. B **87**, 104510 (2013).

[9] E. M. Choi, H.-J. Kim, S. K. Gupta, P. Chowdhury, K. H. P. Kim, S.-I. Lee, W. N. Kang, H.-J. Kim, M.-H. Jung, and S.-H. Park, Effect of two bands on the scaling of critical current density in MgB_2 thin films, Phys. Rev. B **69**, 224510 (2004).

[10] J. Hanisch, K. Iida, S. Haindl, F. Kurth, A. Kauffmann, M. Kidszun, T. Thersleff, J. Freudenberger, L. Schultz, and B. Holzapfel, j_c scaling and anisotropies in Co-doped Ba-122 thin films, IEEE Trans. Appl. Supercond. **21**, 2887 (2011).

[11] Z. Cheng, C. Dong, H. Huang, S. Liu, Y. Zhu, D. Wang, V. Vlasko-Vlasov, U. Welp, W.-K. Kwok, and Y. Ma, Chemical stability and superconductivity in Ag-sheathed $CaKFe_4As_4$ superconducting tapes, Supercond. Sci. Technol. **32**, 015008 (2018).

[12] M. P. Smylie, M. Leroux, V. Mishra, L. Fang, K. M. Taddei, O. Chmaissem, H. Claus, A. Kayani, A. Snezhko, U. Welp, and W.-K. Kwok, Effect of proton irradiation on superconductivity in optimally doped $BaFe_2(As_{1-x}P_x)_2$ single crystals, Phys. Rev. B **93**, 115119 (2016).

[13] S. Pyon, D. Miyawaki, I. Veshchunov, T. Tamegai, K. Takano, H. Kajitani, N. Koizumi, and S. Awaji, Fabrication and characterization of $CaKFe_4As_4$ round wires sintered at high pressure, Appl. Phys. Express **11**, 123101 (2018).

[14] Z. Cheng, S. Liu, C. Dong, H. Huang, L. Li, Y. Zhu, S. Awaji, and Y. Ma, Effects of core density and impurities on the critical current density of $CaKFe_4As_4$ superconducting tapes, Supercond. Sci. Technol. **32**, 105014 (2019).

[15] W. R. Meier, T. Kong, U. S. Kaluarachchi, V. Taufour, N. H. Jo, G. Drachuck, A. E. Böhmer, S. M. Saunders, A. Sapkota, A. Kreyssig, M. A. Tanatar, R. Prozorov, A. I. Goldman, F. F. Balakirev, A. Gurevich, S. L. Bud'ko, and P. C. Canfield, Anisotropic thermodynamic and transport properties of single-crystalline $CaKFe_4As_4$, Phys. Rev. B **94**, 064501 (2016).

[16] G. Ghigo, G. A. Ummarino, L. Gozzelino, R. Gerbaldo, F. Laviano, D. Torsello, and T. Tamegai, Effects of disorder induced by heavy-ion irradiation on $(Ba_{1-x}K_x)Fe_2As_2$ single crystals, within the three-band Eliashberg $s_\pm$ wave model, Sci. Rep. **7**, 13029 (2017).

[17] G. Ghigo, D. Torsello, R. Gerbaldo, L. Gozzelino, F. Laviano, and T. Tamegai, Effects of heavy-ion irradiation on the microwave surface impedance of $(Ba_{1-x}K_x)Fe_2As_2$ single crystals, Supercond. Sci. Technol. **31**, 034006 (2018).

[18] G. Ghigo, D. Torsello, G. A. Ummarino, L. Gozzelino, M. A. Tanatar, R. Prozorov, and P. C. Canfield, Disorder-Driven Transition from $s_\pm$ to s_{++} Superconducting Order Parameter in Proton Irradiated $Ba(Fe_{1-x}Rh_x)_2As_2$ Single Crystals, Phys. Rev. Lett. **121**, 107001 (2018).

[19] G. Ghigo, D. Torsello, L. Gozzelino, T. Tamegai, I. S. Veshchunov, S. Pyon, W. Jiao, G.-H. Cao, S. Y. Grebenchuk, I. A. Golovchanskiy, V. S. Stolyarov, and D. Roditchev, Microwave analysis of the interplay between magnetism and superconductivity in $EuFe_2(As_{1-x}P_x)_2$ single crystals, Phys. Rev. Res. **1**, 033110 (2019).

[20] G. Ghigo, G. A. Ummarino, L. Gozzelino, and T. Tamegai, Penetration depth of $Ba_{1-x}K_xFe_2As_2$ single crystals explained within a multiband Eliashberg $s_\pm$ approach, Phys. Rev. B **96**, 014501 (2017).

[21] T. Sato, K. Niita, N. Matsuda, S. Hashimoto, Y. Iwamoto, S. Noda, T. Ogawa, H. Iwase, H. Nakashima, T. Fukahori, K. Okumura, T. Kai, S. Chiba, T. Furuta, and L. Sihver, Particle and heavy ion transport code system, PHITS, version 2.52, J. Nucl. Sci. Technol. **50**, 913 (2013).

[22] J. F. Ziegler, M. Ziegler, and J. Biersack, SRIM—the stopping and range of ions in matter (2010), Nucl. Instrum. Meth. B **268**, 1818 (2010).

[23] X. Gonze *et al.*, Recent developments in the ABINIT software package, Comput. Phys. Commun. **205**, 106 (2016).

[24] D. Torsello, G. A. Ummarino, L. Gozzelino, T. Tamegai, and G. Ghigo, Comprehensive Eliashberg analysis of microwave conductivity and penetration depth of K-, Co-, and P-substituted $BaFe_2As_2$, Phys. Rev. B **99**, 134518 (2019).

[25] G. A. Ummarino, D. Daghero, M. Tortello, and R. S. Gonnelli, Predictions of multiband $s_\pm$ strong-coupling Eliashberg theory compared to experimental data in iron pnictides, J. Supercond. Novel Magn. **24**, 247 (2011).

[26] D. Mou, T. Kong, W. R. Meier, F. Lochner, L.-L. Wang, Q. Lin, Y. Wu, S. L. Bud'ko, I. Eremin, D. D. Johnson, P. C. Canfield, and A. Kaminski, Enhancement of the Superconducting Gap by Nesting in $CaKFe_4As_4$: A New High Temperature Superconductor, Phys. Rev. Lett. **117**, 277001 (2016).

[27] D. Torsello, G. A. Ummarino, R. Gerbaldo, L. Gozzelino, and G. Ghigo, Eliashberg analysis of the electrodynamic response of $Ba(Fe_{1-x}Rh_x)_2As_2$ the $s_\pm$ to s_{++} order parameter transition, J. Supercond. Novel Magn (2019).

[28] O. V. Dolgov, A. A. Golubov, and D. Parker, Microwave response of superconducting pnictides: Extended $s_\pm$ scenario, New J. Phys. **11**, 075012 (2009).

[29] D. Torsello, K. Cho, K. R. Joshi, S. Ghimire, G. A. Ummarino, N. M. Nusran, M. A. Tanatar, W. R. Meier, M. Xu, S. L. Bud'ko, P. C. Canfield, G. Ghigo, and R. Prozorov, Analysis of the London penetration depth in Ni-doped $CaKFe_4As_4$, Phys. Rev. B **100**, 094513 (2019).

[30] H. Hosono, A. Yamamoto, H. Hiramatsu, and Y. Ma, Recent advances in iron-based superconductors toward applications, Mater. Today **21**, 278 (2018).

[31] S. Pyon, T. Suwa, A. Park, H. Kajitani, N. Koizumi, Y. Tsuchiya, S. Awaji, K. Watanabe, and T. Tamegai, Enhancement of critical current densities in (Ba, K)Fe_2As_2 wires and tapes using HIP technique, Supercond. Sci. Technol. **29**, 115002 (2016).

[32] K. Iida, H. Sato, C. Tarantini, J. Hänisch, J. Jaroszynski, H. Hiramatsu, B. Holzapfel, and H. Hosono, High-field transport properties of a P-doped $BaFe_2As_2$ film on technical substrate, Sci. Rep. **7**, 39951 (2017).

[33] N. Haberkorn, M. Xu, W. R. Meier, S. Suárez, S. L. Bud'ko, and P. C. Canfield, Enhancement of critical current density in $CaKFe_4As_4$ single crystals through 3 MeV proton irradiation, Supercond. Sci. Technol. **33**, 025008 (2020).

[34] C. J. van der Beek, M. Konczykowski, and R. Prozorov, Anisotropy of strong pinning in multi-band superconductors, Supercond. Sci. Technol. **25**, 084010 (2012).

[35] G. Blatter, V. B. Geshkenbein, and A. I. Larkin, From Isotropic to Anisotropic Superconductors: A Scaling Approach, Phys. Rev. Lett. **68**, 875 (1992).

[36] C. Tarantini, K. Iida, J. Hänisch, F. Kurth, J. Jaroszynski, N. Sumiya, M. Chihara, T. Hatano, H. Ikuta, S. Schmidt, *et al.*, Intrinsic and extrinsic pinning in NdFeAs(O,F): Vortex trapping and lock-in by the layered structure, Sci. Rep. **6**, 36047 (2016).

[37] M. Kończykowski, C. J. van der Beek, M. A. Tanatar, V. Mosser, Y. J. Song, Y. S. Kwon, and R. Prozorov, Anisotropy of the coherence length from critical currents in the stoichiometric superconductor LiFeAs, Phys. Rev. B **84**, 180514 (2011).

[38] A. Takahashi, S. Pyon, S. Okayasu, S. Ishida, A. Iyo, H. Eisaki, M. Imai, H. Abe, T. Terashima, and T. Tamegai, Effects of swift-particle irradiations on critical current density in $CaKFe_4As_4$, J. Phys.: Conf. Ser. **1293**, 012013 (2019).

[39] L. Salasnich, A. A. Shanenko, A. Vagov, J. A. Aguiar, and A. Perali, Screening of pair fluctuations in superconductors with coupled shallow and deep bands: A route to higher-temperature superconductivity, Phys. Rev. B **100**, 064510 (2019).

[40] M. W. Rupich, S. Sathyamurthy, S. Fleshler, Q. Li, V. Solovyov, T. Ozaki, U. Welp, W.-K. Kwok, M. Leroux, A. E. Koshelev, *et al.*, Engineered pinning landscapes for enhanced 2G coil wire, IEEE Trans. Appl. Supercond. **26**, 1 (2016).

[41] M. Leroux, K. J. Kihlstrom, S. Holleis, M. W. Rupich, S. Sathyamurthy, S. Fleshler, H. Sheng, D. J. Miller, S. Eley, L. Civale, *et al.*, Rapid doubling of the critical current of $YBa_2Cu_3O_7 - \delta$ coated conductors for viable high-speed industrial processing, Appl. Phys. Lett. **107**, 192601 (2015).

[42] T. Ozaki, L. Wu, C. Zhang, W. Si, Q. Jie, and Q. Li, Enhanced critical current in superconducting $FeSe_{0}.5Te_{0}.5$ films at all magnetic field orientations by scalable gold ion irradiation, Supercond. Sci. Technol. **31**, 024002 (2018).